Experimental demonstration of underwater acoustic communication by vector sensors

Aijun Song, Ali Abdi, Mohsen Badiey, and Paul Hursky

Abstract

Acoustic communication often relies on a large size array with multiple spatially separated hydrophones to deal with the challenging underwater channel. This poses limitation to its application in compact size underwater platforms. In this paper, acoustic communication by vector sensors is demonstrated by the data collected during a high frequency acoustic experiment, where a vector sensor array was drifting in the ocean. It is shown that the multichannel receiver using a single vector sensor can offer significant size reduction for coherent acoustic communication at the carrier frequency of 12 kHz, compared with a pressure sensor line array. Further, the performance difference between vector sensors and pressure sensors varies at communication ranges. At close ranges (up to 160 m), both a single vector sensor and a vector sensor array can offer significant performance gain compared with the pressure sensor array. At longer ranges (up to 1080 m), the single vector sensor has the same performance with the pressure sensor array, on average. The vector sensor array consistently provides gain at all ranges over the pressure sensor array since additional information of the acoustic field is utilized by vector sensors.

This work was supported by the Office of Naval Research (ONR) Code 321OA (Grant No. N00014-01-1-0114) and the National Science Foundation (NSF) (Grant No. CCF-0830204 and CCF-0830190). Part of the content has been presented to the OCEANS'08 meeting, Quebec, Canada, Sept. 15-18, 2008.

Aijun Song and Mohsen Badiey are with College of Earth, Ocean, and Environment, University of Delaware, 114 Robinson Hall, Newark, DE 19716. Ali Abdi is with Center for Wireless Communications and Signal Processing Research, Electrical & Computer Engineering Department, New Jersey Institute of Technology, Newark, NJ, 07102. Pual Hursky is with Heat, Light, and Sound Research, Inc., 3366 North Torrey Pines Ct., La Jolla, CA 92037

I. INTRODUCTION

Underwater acoustic communication is critical to a number of civilian and scientific missions in the ocean, for example navigation and communication for underwater autonomous vehicles (AUVs). However, the underwater channel is challenging for digital communication [1]. To deal with significant multipath and fast channel fluctuations, reception diversity from spatially separated hydrophones is often employed to achieve acceptable performance. Readers can refer to [2]–[4] for multichannel decision feedback equalization (DFE) and [5]–[10] for time reversal methods as design examples. These designs often lead to the usage of a large size array, which might be impossible to accommodate at compact underwater platforms such as AUVs. Moreover, smaller array size is always preferred in underwater missions because it leads to easier operations. In this paper, we explore the possibilities of using vector sensors as an alternative to spatially separated pressure sensors.

Acoustic vector sensors are capable of measuring three orthogonal particle velocity components of the acoustic field, in addition to the scalar acoustic pressure, at a collocated point in space [11]. They have long been considered for localization and detection of underwater objects [11]–[15]. For example, four physical quantities measured by a vector sensor have been processed by a multichannel filter to perform beamforming [16]–[18]. Vector sensors and vector sensor arrays can offer improved performance in direction-finding applications compared with their scalar pressure counterparts [18]. It has been proposed in [19] that a single vector can serve as a multichannel receiver for underwater digital communication through the use of both scalar pressure and particle velocity components of the acoustic field. Multiuser communication with vector sensor has been investigated through computer simulations in [20]. Motivated by the potential applications of vector sensors in underwater communication, statistical correlation models for acoustic vector sensor arrays have been developed in [21].

In this paper, we use the experimental data to demonstrate the usefulness of velocity channels for acoustic communication. Both a single vector sensor and an array of vector sensors are investigated for coherent acoustic communication using experimental data. The paper is organized as follows. System equations for communication by vector sensors are briefly reviewed in Section II. Channel properties

and computer simulations for the usage of vector sensors in coherent underwater communication are discussed in Section III. Experimental demonstration of the concept is provided in Section IV and concluding remarks are given in Section V.

II. System Equations

In this section, basic system equations for data detection via a vector sensor introduced in [22] are briefly reviewed. To demonstrate the basic concepts of how both the vector and scalar components of the acoustic field can be utilized for data reception, we consider a simple system with one transducer and one vector sensor. As shown in Fig. 1, the vector sensor denoted as a black square measures the pressure and the x, y, and z components of the particle velocity.

A. Pressure and Velocity Channels and Noise

There are four channels in Fig. 1: the pressure channel p, represented by a straight dashed line, and three pressure-equivalent velocity channels p^x, p^y, and p^z, shown by curved dashed lines. To define p^x, p^y, and p^z, we first define the particle velocities, v^x, v^y and v^z. According to the linearized equation for time-harmonic waves, the x, y and z components of the velocity at the frequency f_0 are given by [23]:

$$\begin{aligned} v^x &= -(j\rho_0\omega_0)^{-1}\partial p/\partial x, \\ v^y &= -(j\rho_0\omega_0)^{-1}\partial p/\partial y, \\ v^z &= -(j\rho_0\omega_0)^{-1}\partial p/\partial z, \end{aligned} \tag{1}$$

where ρ_0 is the density of the fluid, and $j = \sqrt{-1}$. Eq.(1) states that the velocity in a certain direction is proportional to the spatial pressure gradient in that direction [23]. The associated pressure-equivalent velocity channels are defined as $p^x = -\rho_0 c v^x$, $p^y = -\rho_0 c v^y$ and $p^z = -\rho_0 c v^z$, which give

$$\begin{aligned} p^x &= (jk)^{-1}\partial p/\partial x, \\ p^y &= (jk)^{-1}\partial p/\partial y, \\ p^z &= (jk)^{-1}\partial p/\partial z, \end{aligned} \tag{2}$$

where $k = \omega_0/c$ is the acoustic wavenumber and c is the sound speed.

The additive ambient noise pressure at the receiver is shown by w in Fig. 1. Similar to Eq. (1), the x, y, and z components of ambient noise velocities are $\alpha^x = -(j\rho_0\omega_0)^{-1}\partial w/\partial x$, $\alpha^y = -(j\rho_0\omega_0)^{-1}\partial w/\partial y$, and $\alpha^z = -(j\rho_0\omega_0)^{-1}\partial w/\partial z$, respectively. So we can obtain the pressure-equivalent ambient noise velocities as

$$\begin{aligned} w^x &= (jk)^{-1}\partial w/\partial x, \\ w^y &= (jk)^{-1}\partial w/\partial y, \\ w^z &= (jk)^{-1}\partial w/\partial z. \end{aligned} \tag{3}$$

B. Input-Output System Equations

According to Fig. 1, the received pressure signal r in response to the signal s transmitted from the transmitter can be written as $r = p \circledast s + w$. Here $\circledast$ stands for convolution in time and p is the pressure channel impulse response. We also define the pressure-equivalent received velocity signals as $r^x = (jk)^{-1}\partial r/\partial x$, $r^y = (jk)^{-1}\partial r/\partial y$, and $r^z = (jk)^{-1}\partial r/\partial z$. Based on (2) and by taking the spatial gradient with respect to x, y, and z axes, we obtain key system equations

$$\begin{aligned} r &= p \circledast s + w, \\ r^x &= p^x \circledast s + w^x, \\ r^y &= p^y \circledast s + w^y, \\ r^z &= p^z \circledast s + w^z. \end{aligned} \tag{4}$$

Note that the four output signals are measured at a collocated point in space. With the assumption that the noise is spherically isotropic, the noise terms in Eq.(4) are uncorrelated [14]. In addition to the noise correlation property, the arrival structure and correlation functions of the channels are relevant to acoustic communication performance. As shown by the numerical acoustic simulations in [19], [22], the pressure channel and the velocity channels can provide a new form of diversity, similar to an array of spatially separated pressure sensors. Therefore, the pressure source and vector sensor in Fig. 1 have the potential to form a single-input multiple-output (SIMO) system. In the next section, relevant channel characteristics are reported including delay spread, noise correlation, and channel correlation from experimental data.

III. MEASURED CHANNEL CHARACTERISTICS

During a high frequency Makai acoustic communication experiment (MakaiEx) conducted west off the Kauai Island, Hawaii, in September and October of 2005 [24], a five element Wilcoxon array was deployed multiple times. The measured characteristics of particle velocity channels are presented in this section. The performance of particle velocity channels in digital communication is investigated by computer simulations to gain some initial insight in this section. Performance obtained from at-sea experiments will be discussed in Section IV.

A. Channel measurements during MakaiEx

Each element of the Wilcoxon vector sensor array had three velocity-meters that were sensitive only along a specific direction, besides an embedded omni-directional pressure sensor [15]. Therefore, each vector sensor had four channels and generated four data streams: one pressure channel and three x, y, and z components of the particle velocity. The length of each vector sensor was 6.6 cm, and the element spacing (center-to-center distance) was 10 cm. In one deployment on September 23, 2005, a bottom mounted acoustic source continuously transmitted a series of communication signals at the carrier frequency of $f_0 = 12$ kHz. The water depth at the source was about 100 m and the source depth was about 95 m. The vector sensor array was attached to A-frame steel cable of the drifting R/V Kilo Moana. The array was considered vertical since a 200 pound weight was attached to the end of the array cable. The top element is referred to as the first. The bottom element, or the fourth, was about 40 m below the sea surface. During the experiment, the R/V Kilo Moana was drifting in deeper water.

As mentioned, a pressure source and a vector sensor can form a 1×4 SIMO communication system, similar to four pressure channels of four vector sensors. Note the four channels of a vector sensor are co-located at a single point in space, whereas the four pressure channels have an aperture of 30 cm. In what follows, channel characteristics and receiver performance of these two systems are compared. Fig. 2 shows an example of the impulse response functions obtained from the field data. A pseudo random BPSK signal at the carrier frequency of $f_0 = 12$ kHz was used to probe the impulse responses during the experiment. The symbol rate of the BPSK signal was 6 kilosymbols/s

and the utilized bandwidth was 6 kHz. The impulse response was obtained by the least squares channel estimation algorithm. For this particular dataset, the source-receiver range was about 20 m. The range was calculated based on the ship GPS data and source position. As shown in Fig. 2(a), the x-, y-, and z- particle velocity channels had an arrival structure similar to the pressure channel. However, later arrivals of y and z particle velocity channels were weaker. This resulted in smaller root-mean-square (RMS) delay spreads, which is defined as [25]

$$\tau_{rms} = \sqrt{\frac{\sum_l (lT_s)^2 |h(l)|^2}{\sum_l |h(l)|^2} - \left(\frac{\sum_l (lT_s)|h(l)|^2}{\sum_l |h(l)|^2} \right)^2}, \tag{5}$$

where $h(l)$ is a discrete, baseband impulse response sampled at a period of T_s. Specifically, the delay spread of the pressure channel was 3.9 ms, whereas those of the x, y and z channels were 4.6 ms, 2.0 ms and 2.6 ms, respectively. Considering the 30 cm aperture of the pressure sensor line array, the four pressure channel impulse responses showed similarity among themselves, as demonstrated in Fig. 2(b). The delay spread of the four pressure channels were 3.7 ms, 4.3 ms, 5.2 ms, and 4.6 ms, respectively. Since a small delay spread corresponds to less inter-symbol interference (ISI), the y- and z- velocity channels might offer better communication results than the pressure channels [19].

Besides the delay spread, channel/noise correlations are also relevant to the receiver performance. Table I shows the noise and channel correlation among the multiple channels of the vector sensor and of the pressure sensor line array. The correlation numbers in Table I are the modulus of the complex correlation defined as

$$\gamma_{m,l} = \left| \frac{E[u_m u_l^*] - E[u_m]E[u_l^*]}{\sqrt{(E[|u_m|^2] - |E[u_m]|^2)(E[|u_l|^2] - |E[u_l]|^2)}} \right|, \tag{6}$$

where u_m, u_l are two complex sequences and $E[\cdot]$ represents the expectation operation. The channel impulse responses shown in Fig. 2 were used for the correlation calculation. For the vector sensor, the pressure, x-velocity, y-velocity, and z-velocity channels of the first sensor were numbered as channel #1 to channel #4, respectively. The pressure outputs of the four vector sensors were used in the correlation analysis of the pressure sensor array. The noise correlation calculation used 3.75 s ambient noise, which was recorded 20 seconds before the BPSK training sequence.

As shown in Table I, although the four channels of the vector sensor were co-located at a single

point, correlation among some of the channels could be small. Further, most of the noise correlation numbers of the vector sensor were smaller than those of the pressure sensor array.

B. Simulated performance of vector sensor receivers

In Fig.3, the bit-error-rates (BERs) of the receivers using a single vector sensor, a single pressure sensor, and a four-element pressure sensor array are shown. The experimental impulse responses shown in Fig. 2 were used. The classic symbol-spaced DFE was used to compensate for the ISI in a single channel as well as in multiple channels [2], [26]. Carrier phase offset and time variation of the channel were not considered. The number of the feedforward taps was $N_{ff} = 600$ for the multichannel DFE and the number of the feedback taps was $N_{fb} = 149$ symbols. The BERs corresponded to a 6 kilobits/s uncoded BPSK data stream at $f_0 = 12$ kHz. As expected, the y-velocity channel receiver had about 1 dB reduction in the required signal-to-noise ratio (SNR) over the single pressure sensor receiver for the BER of 10^{-4}. This was attributed to the smaller delay spread of the y-velocity channel. By using all the channels of the vector sensor, a 7 dB reduction in the required SNR for the BER of 10^{-4} could be obtained, compared with a single pressure sensor receiver. The vector sensor receiver showed modest improvement (1.5 dB) over the four-channel pressure sensor array. The average SNR of each multichannel receiver is defined as [19]

$$\rho = (\Omega_p/\Omega_w + \Omega_p^x/\Omega_w^x + \Omega_p^y/\Omega_w^y + \Omega_p^z/\Omega_w^z)/4, \tag{7}$$

where Ω_p, Ω_p^x, Ω_p^y, and Ω_p^z are the average powers of the pressure channel and of the particle velocity channels, and Ω_w, Ω_w^x, Ω_w^y, and Ω_w^z are their respective noise powers.

The vector sensor had a compact size (6.6 cm) compared with the 30 cm pressure sensor array. This is crucial in acoustic modem applications for AUVs where there are serious limitations on receiver size. This benefit is the result of the co-located particle velocity information that can be measured by a compact vector sensor. This is an alternative to spatially separated pressure sensors to achieve reception diversity.

IV. COMMUNICATION EXPERIMENT USING VECTOR SENSORS

In this section, we present a practical receiver to utilize particle velocity channels in the underwater environment. Experimental data collected at multiple communication ranges are analyzed. Performance comparison between vector sensors and a pressure sensor array is reported as well.

A. Multichannel equalizer to utilize the particle velocity channels

Considering the time-varying, dispersive properties of the underwater channel, Eq. (4) can be re-written for a receiver with M multiple vector sensors as

$$r_i(n) = e^{j\theta_i(n)} \left[h_i(n,l) \circledast s(n)\right] + w_i(n), \quad i = 1 \text{ to } I = 4M, \tag{8}$$

where the pressure channel, x-velocity channel, y-velocity channel, and z-velocity channel of the m-th vector sensor, $m = 1, \cdots, M$, correspond to channel indexes $4(m-1)+1$ to $4m$. In Eq. (8), $\theta_i(n)$ is the instantaneous carrier phase offset. $h_i(n,l)$, $0 \le l \le L-1$, is the discrete-time baseband impulse response function where L is the impulse response length in symbols. Note that Eq. (8) can also be used as the input-output equation for an I-element pressure sensor array.

Figure 4 shows the receiver structure, which is similar to the algorithm presented in [4]. As a channel-estimation-based processor, the multichannel equalizer tracks channel and carrier phase variations to accommodate fast channel variations. The channel estimate $\hat{h}_i(n,l)$ can be obtained from the received signal and the past decision results $\hat{s}(n)^{past}$ using the least squares method [27]. The receiver consists of four components: noise normalization, phase tracking and correction, time reversal multichannel combining, and finally a single channel DFE. A noise normalization component is needed since the noise power usually is not uniformly distributed among the pressure channel and the velocity channels [14]. The noise power in the channel estimator [27] can be used as an estimate of the noise power

$$\hat{\sigma}_i^2 = \frac{\sum_{n=1}^{N_0} \left| r_i(n) - \hat{h}_i(n,l) \circledast s(n)^{preamble} \right|^2}{N_0 - L}, \tag{9}$$

where $s(n)^{preamble}$ is the source symbol of the preamble and N_0 is channel estimation block size.

After noise normalization, time reversal multichannel combining uses time reversed channel estimates $(\hat{h}_i(n,-l))^*$ as matched-filters for the phase-corrected signals $z_i(n)$ on each channel [28]. The

output after time reversal combining is

$$\begin{aligned} c(n) &= \sum_{i=1}^{I} (\hat{h}_i(n,-l))^* \circledast z_i(n) \\ &= s(n) \circledast q(n,l) + w'(n), \end{aligned} \tag{10}$$

where $w'(n)$ is the combined noise term and $q(n,l)$ is the effective impulse response between the source and output of time reversal.

After time reversal, a single channel DFE with joint phase tracking [2] is used to compensate for the residual ISI and phase fluctuations in $c(n)$. The exponentially weighted recursive least-squares (RLS) algorithm is used to update the equalizer tap weights. The mean square error at the soft output of the DFE, $\tilde{s}(n)$, and the BER of the hard decision, $\hat{s}(n)$, are used as performance metrics in the next subsection.

The receiver in Fig. 4 is equivalent to the optimal multichannel DFE structure [2]. Rather than applying feedforward filters to the individual channels, the proposed receiver uses a single channel DFE on the composite channel after time reversal combining. The proposed receiver avoids, explicit or inexplicit, calculation and updating of large number of feedforward filters for individual channels. The length of the single channel DFE filters in the proposed receiver are shorter since the effective impulse response $q(n,l)$ is usually compact and near time-invariant. This lead to low complexity of the proposed receiver in the time-varying, dispersive underwater channel.

B. Communication data analysis

In Section III, the impulse responses at the communication range of 20 m were presented for the particle velocity channels. In this section, communication data from seven source-receiver ranges up to 1 km are analyzed. A uniform set of receiver parameters were used to demodulate all the BPSK data including the measurements from pressure channels as well as from particle velocity channels. The received data were over-sampled with an over-sampling rate of $K = 3$. The estimated channel length was 25 ms or $L = 150$ symbols. The channel estimation block size was chosen to be three times of the channel length, i.e., $N_0 = 3L$. The number of the feedforward taps was $KN_{ff} = 45$ for the fractionally spaced DFE, where $N_{ff} = 15$ was the feedforward filter span in symbols. The

number of the feedback taps was $N_{fb} = 5$ symbols. At the beginning of the 3.75 s BPSK packet, $N_p = 1600$ symbols were used for noise normalization, initial channel estimation, phase tracking, and DFE tap weight training. The RLS forgetting factor λ in the DFE was 0.999.

For seven BPSK transmissions at different ranges, the demodulation results are shown in Table II. The time reversal receiver in Fig. 4 was applied to four channels of a single vector sensor, the four pressure channels of the four vector sensors (a pressure sensor array), and 16 channels of the four vector sensors (a vector sensor array). The receiver used previous detected symbols for channel estimation and equalization after the preamble. It is noted that there was no difference in the observed phase offset between the particle velocity channel and the pressure channels. This is consistent with the theoretical analysis in [29], where it is shown that Doppler spreads of particle velocity and pressure channels are nearly the same. When there were excessive errors for a demodulation block, for example BER greater than 0.3, the receiver would not be able to estimate the channel. We then consider this as receiver failure as marked in Table II for several cases. The average channel delay spread and average correlation coefficients are listed for each range in Table III. The average was calculated over the 3.75 s BPSK packet.

The results can be discussed into three range groups. The first group includes the close range (20, 80, and 160 m). The receivers using vector sensors had significant performance advantage at these close communication ranges. For example, at the 20 and 80 m range, the single vector sensor receiver had about 5.5 and 2.5 dB reduction in the output MSE over the pressure sensor receiver. At 160 m, the pressure sensor array receiver failed whereas the single vector sensor had an output MSE of -4.7 dB.

At these ranges, the direct path was strong and multipath effect was limited due to the close range. The channels were very similar to impulse responses shown in Fig. 2. For the vector sensor, the y- and z- velocity channels had weaker later arrivals reflected as smaller delay spread of y- and z-velocity channels in Table III for these ranges. The performance gain was partially attributed to the smaller delay spread of the y- and z- velocity channels.

For the second range group (290 and 430 m), the pressure sensor array outperformed the single

vector sensor. The receiver with the single vector sensor failed at the 290 m range while the output MSE of the pressure sensor array was -4.8 dB. The performance gain of the pressure sensor array was partly due to lower correlation among its four pressure elements than among the four channels of the vector sensor. At the 430 m range, the pressure sensor array had modest gain over the single vector sensor, 1.4 dB reduction in the output MSE. Note that such gain of the pressure sensor array at these ranges came with the price of the larger size receiving array, compared with a compact vector sensor [22]. At these ranges, the channels had strong multipath and later arrivals fluctuated very fast. As an example, the pressure and velocity channels of a vector sensor at the 430 m range are shown in Fig. 5. The velocity channels did not have the advantage of smaller delay spread or lower correlation. However, the vector sensor array had about 1.4 dB improvements over the pressure sensor array in terms of the output MSE.

For the third range group (900 and 1080 m), the single vector sensor performed better than the pressure sensor array: the output MSE was -4.6 dB and -4.1 dB, respectively for these two ranges, for the single vector sensor while the receiver with the pressure sensor array failed. This was due to the high correlation (close to 0.9 and higher) among all the channels of the pressure sensor array at these two ranges, as listed in Table III. The vector sensor array performed similarly to a single vector sensor, confirming strong correlation among the corresponding channels from multiple elements of the array.

V. Conclusion

In this paper, particle velocity channels provided by vector sensors were utilized for underwater acoustic communication. Through the use of the MakaiEx data, coherent communication by vector sensors was demonstrated between a bottom mounted sound source and a drifting vector sensor vertical array. A practical multichannel equalizer with near-optimal performance was implemented to process the data at multiple communication ranges. Channel parameters such as correlation and delay spread that affect data communication were calculated from the measurements. It was shown that the multichannel equalizer using a single vector sensor can offer significant receiver size reduction for coherent acoustic communication at the carrier frequency of 12 kHz, compared with a 30 cm aperture

pressure sensor line array. Further, the performance difference between vector sensors and pressure sensors varied at communication ranges. At close ranges (up to 160 m), both a single vector sensor and a vector sensor array offered significant performance gain compared with the pressure sensor array. At longer ranges (up to 1080 m), the vector sensor array provided consistent performance gain, although smaller than those at close ranges, over the pressure sensor array since additional information of the acoustic field was utilized. These results suggest that vector sensors can offer acoustic communication solutions that are particularly needed in the compact underwater platforms.

ACKNOWLEDGMENT

Authors wish to thank all the participants of MakaiEx. We also wish to give special thanks to Bruce Abraham (Applied Physical Sciences), who participated in the vector sensor experiment as part of MakaiEx.

REFERENCES

[1] D. B. Kilfoyle and A. B. Baggeroer, "The state of the art in underwater acoustic telemetry," *IEEE J. Oceanic Eng.*, vol. 25, no. 1, pp. 4–27, Jan. 2000.

[2] M. Stojanovic, J. Catipovic, and J. G. Proakis, "Adaptive multichannel combining and equalization for underwater acoustic communications," *J. Acoust. Soc. Am.*, vol. 94, no. 3, pp. 1621–1631, Sept. 1993.

[3] M. Stojanovic, J. Catipovic, and J. G. Proakis, "Reduced-complexity spatial and temporal processing of underwater acoustic communication signals," *J. Acoust. Soc. Am.*, vol. 94, no. 2, pp. 961–972, Aug 1995.

[4] A. Song, M. Badiey, H.-C. Song, W. S. Hodgkiss, M. B. Porter, and the KauaiEx Group, "Impact of ocean variability on coherent underwater acoustic communications during the Kauai experiment (KauaiEx)," *J. Acoust. Soc. Am.*, vol. 123, no. 2, pp. 856–865, Feb. 2008.

[5] G. F. Edelmann, T. Akal, W. S. Hodgkiss, S. Kim, W. A. Kuperman, and H. C. Song, "An initial demonstration of underwater acoustic communications using time reversal," *IEEE J. Oceanic Eng.*, vol. 31, no. 3, pp. 602–609, Jul. 2002.

[6] D. Rouseff, D. R. Jackson, W. L. J. Fox, C. D. Jones, J. A. Ritcey, and D. R. Dowling, "Underwater acosutic communication by passive-phase conjugation: Theory and experimental results," *IEEE J. Oceanic Eng.*, vol. 26, no. 4, pp. 821–831, Oct. 2001.

[7] T. C. Yang, "Temporal resolutions of time-reversal and passive-phase conjugation for underwater acoustic communications," *IEEE J. Oceanic Eng.*, vol. 28, no. 2, pp. 229–245, Apr. 2003.

[8] G. F. Edelmann, H. C. Song, S. Kim, W. S. Hodgkiss, W. A. Kuperman, and T. Akal, "Underwater acoustic communications using time reversal," *IEEE J. Oceanic Eng.*, vol. 30, no. 4, pp. 852–864, Oct. 2005.

[9] T. C. Yang, "Correlation-based decision-feedback equalizer for underwater acoustic communications," *IEEE J. Oceanic Eng.*, vol. 30, no. 4, pp. 865–880, Oct. 2005.

[10] H. C. Song, W. S. Hodgkiss, W. A. Kuperman, M. Stevenson, and T. Akal, "Improvement of time reversal communications using adaptive channel equalizers," *IEEE J. Oceanic Eng.*, vol. 31, no. 2, pp. 487–496, Apr. 2006.

[11] A. Nehorai and E. Paldi, "Acoustic vector-sensor array processing," *IEEE Trans. Signal Process.*, vol. 42, no. 9, pp. 2481–2491, Sep. 1994.

[12] K. T. Wong and M. D. Zoltowski, "Closed-form underwater acoustic direction-finding with arbitrarily spaced vector-hydrophones at unknown locations," *IEEE J. Oceanic Eng.*, vol. 22, no. 3, pp. 566–575, Jul. 1997.

[13] M. Hawkes and A. Nehorai, "Acoustic vector-sensor beamforming and Capon direction estimation," *IEEE Trans. Signal Process.*, vol. 46, no. 9, pp. 2291–2304, Sept. 1998.

[14] M. Hawkes and A. Nehorai, "Acoustic vector-sensor correlations in ambient noise," *IEEE J. Oceanic Eng.*, vol. 26, no. 3, pp. 337–347, Jul. 2001.

[15] J. Clay Shipps and B. M. Abraham, "The use of vector sensors for underwater port and waterway security," in *Proc. ISA/IEEE Sensors for Industry Conf.*, New Orleans, LA, 2004.

[16] G. L. D'Spain, W. S. Hodgkiss, and G. L. Edmonds, "The simultaneous measurement of infrasonic acoustic particle velocity and acoustic pressure in the ocean by freely drifting swallow floats," *IEEE J. Oceanic Eng.*, vol. 16, no. 2, pp. 195–207, Apr. 2001.

[17] B. A. Cray and A. H. Nuttall, "Directivity factors for linear arrays of velocity sensors," *J. Acoust. Soc. Am.*, vol. 110, no. 1, pp. 324–331, Jul. 2001.

[18] G. L. D'Spain, J. C. Luby, G. R. Wilson, and R. A. Gramann, "Vector sensors and vector sensor line arrays: Comments on optimal array gain and detection," *J. Acoust. Soc. Am.*, vol. 120, no. 1, pp. 171–185, Jul. 2006.

[19] A. Abdi, H. Guo, and P. Sutthiwan, "A new vector sensor receiver for underwater acoustic communication," in *Proc. Oceans*, Vancouver, Canada, 2007.

[20] H. Guo and A. Abdi, "Multiuser underwater communication with space-time block codes and acoustic vector sensors," in *Proc. Oceans*, Quebec City, Canada, 2008.

[21] A. Abdi and H. Guo, "Signal correlation modeling in acoustic vector sensor arrays," *IEEE Trans. Signal Process.*, vol. 57, no. 3, pp. 892–903, Mar. 2009.

[22] A. Abdi and H. Guo, "A new compact multichannel receiver for underwater wireless communication networks," *IEEE Trans. Wireless Commun.*, vol. 8, no. 7, pp. 3326–3329, Jul. 2009.

[23] A. D. Pierce, *Acoustics: An Introduction to its Physical Principles and Applications*, AIP, Woodbury, New York, 2nd edition, 1989, pp. 14-20.

[24] M. B. Porter *et al.*, "The Makai experiment: High frequency acoustics," in *Proc. European Conf. Underwater Acoustics*, Carvoeiro, Portugal, 2006.

[25] J. D. Parsons, *The Mobile Radio Propagation Channel*, Wiley, New York, 4th edition, 1992, pp. 164-189.

[26] J. G. Proakis, *Digital Communications*, McGraw-Hill, New York, 4th edition, 2000, pp. 638-642.

[27] J. A. Flynn, J. A. Ritcey, D. Rouseff, and W. L. J. Fox, "Multichannel equalization by decision-directed passive phase conjugation: Experimental results," *IEEE J. Oceanic Eng.*, vol. 29, no. 3, pp. 824–836, Jul. 2004.

[28] W. A. Kuperman, W. S. Hodgkiss, H. C. Song, T. Akal, C. Ferla, and D. R. Jackson, "Phase conjuation in the ocean: Experimental demonstration of an acoustic time-reversal mirror," *J. Acoust. Soc. Am.*, vol. 103, no. 1, pp. 25–40, Jan. 1998.

[29] H. Guo, A. Abdi, A. Song, and M. Badiey, "Delay and Doppler spreads in underwater acoustic particle velocity channels," *J. Acoust. Soc. Am.*, 2011, in press.

LIST OF FIGURES

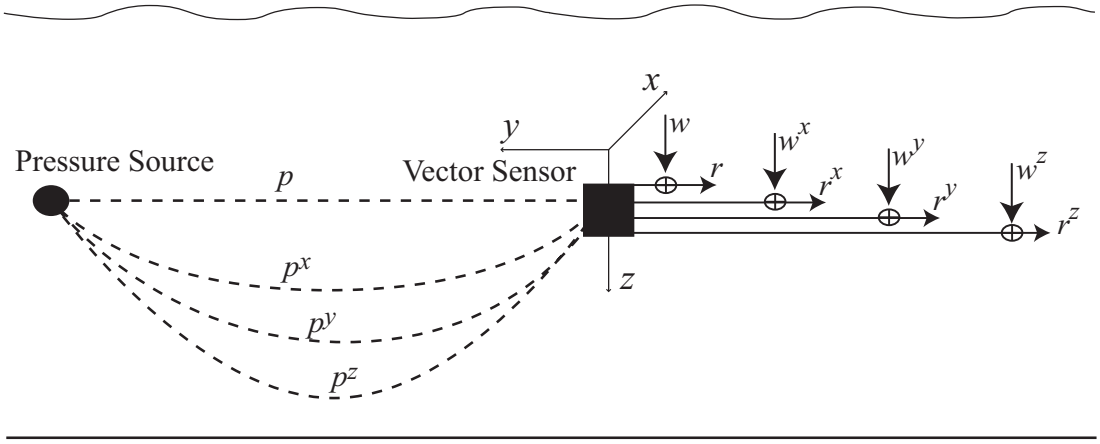

Fig. 1. A 1×4 vector sensor communication system with a sound source and a vector sensor receiver in the underwater environment. The vector sensor measures pressure and x, y, and z components of the acoustic particle velocity, all at a single point in space.

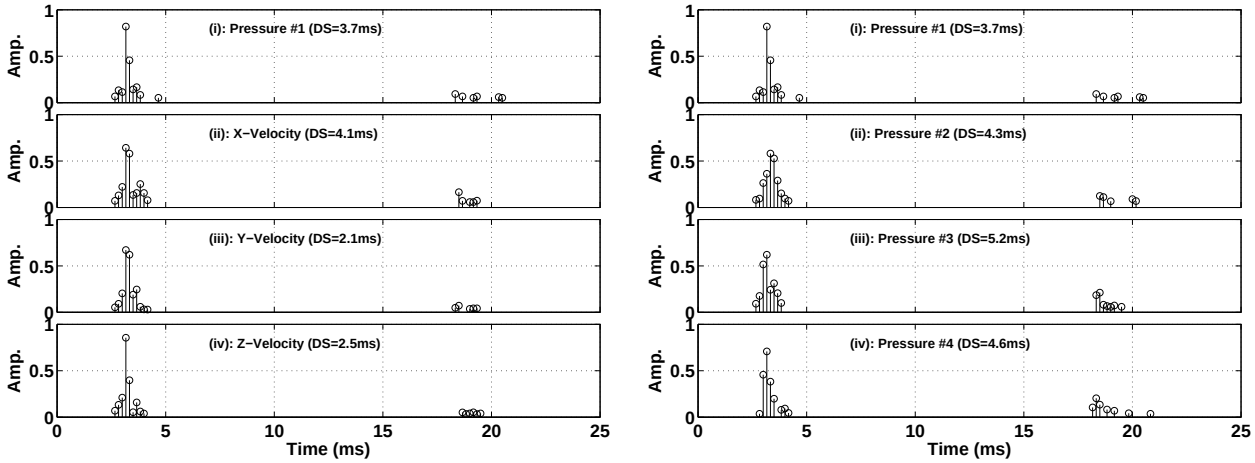

(a) (b)

Fig. 2. Normalized amplitudes of the measured impulse responses (a) from the pressure channel, x-velocity, y-velocity and z-velocity channels of the first sensor; and (b) from the four pressure channels of the array.

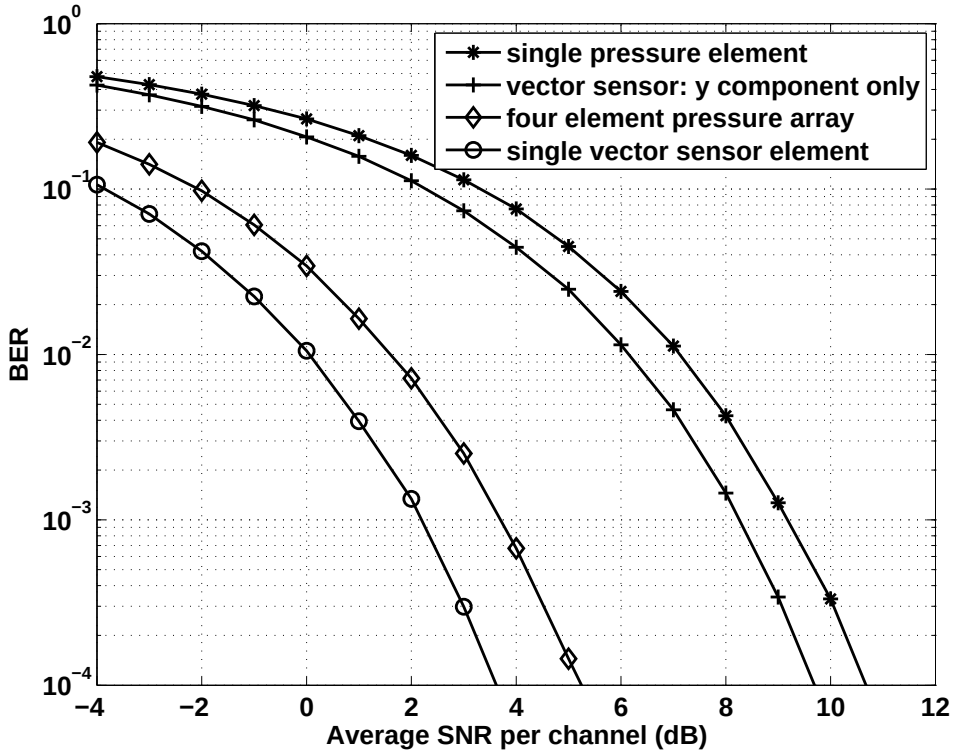

Fig. 3. Simulated performance of the receivers using a single vector sensor, a four-element pressure sensor array, and a single pressure sensor. The impulse responses of Fig. 2 were used. The size of the four element pressure sensor array was 30 cm, whereas the vector sensor size was 6.6 cm.

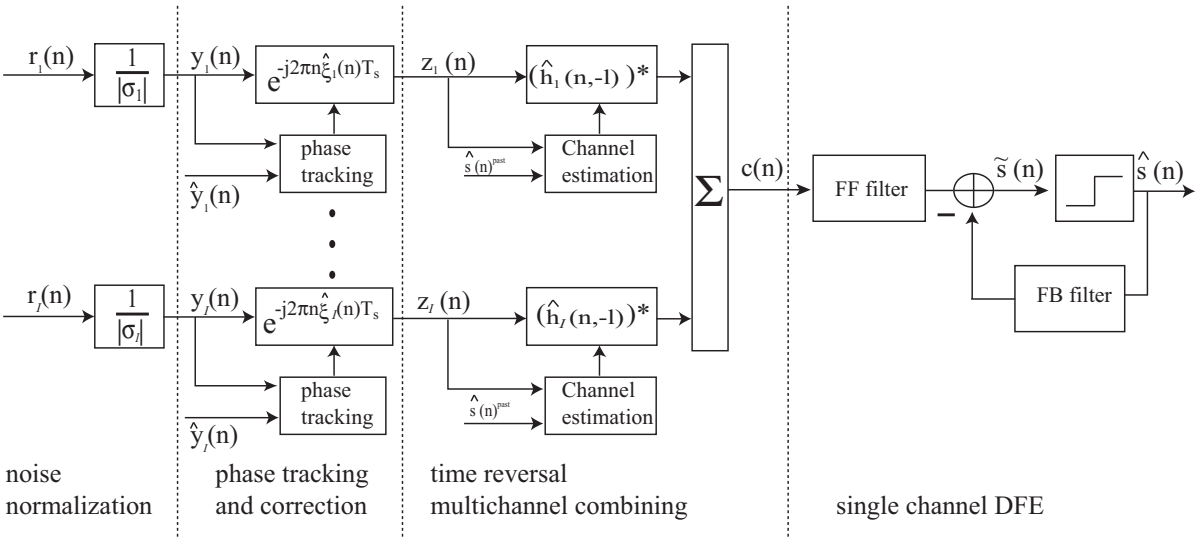

Fig. 4. The practical multichannel equalizer consists of four parts: (1) noise normalization, 2) phase tracking and correction, (3) time reversal multichannel combining, and (4) single channel DFE.

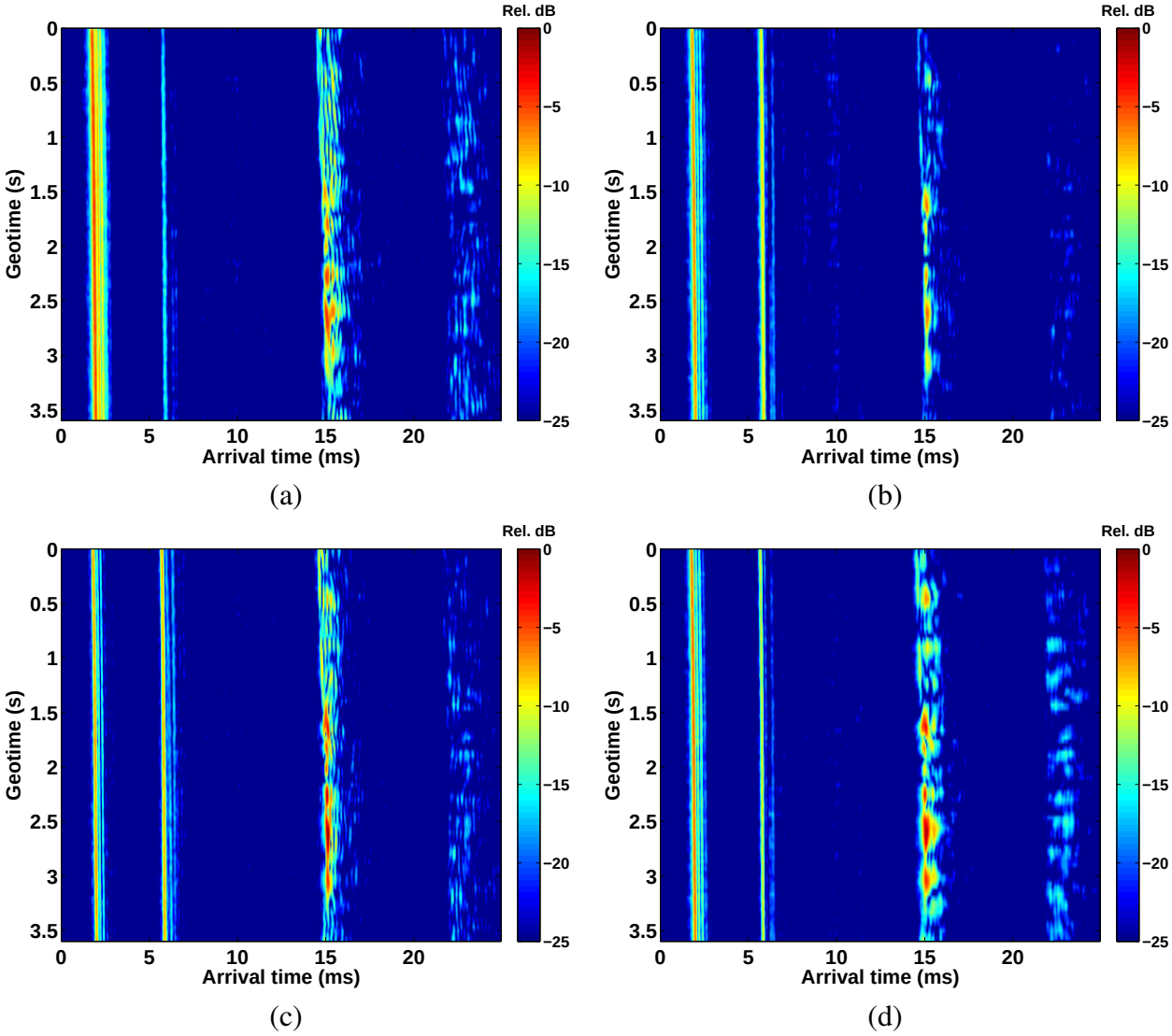

Fig. 5. The measured 3.75 s impulse responses of (a) pressure channel, (b) x-velocity, (c) y-velocity and (d) z-velocity channels at the source-receiver range of about 430 m.

LIST OF TABLES

TABLE I
CHANNEL AND NOISE CORRELATION MEASURED FROM THE FIELD DATA

		Vector Sensor	Pressure Sensor Array
Channel correlation	$\gamma_{1,2}$	0.35	0.45
	$\gamma_{1,3}$	0.81	0.40
	$\gamma_{1,4}$	0.89	0.59
	$\gamma_{2,3}$	0.41	0.46
	$\gamma_{2,4}$	0.40	0.61
	$\gamma_{3,4}$	0.89	0.71
Noise correlation	$\gamma_{1,2}$	0.44	0.67
	$\gamma_{1,3}$	0.53	0.68
	$\gamma_{1,4}$	0.53	0.53
	$\gamma_{2,3}$	0.47	0.56
	$\gamma_{2,4}$	0.21	0.64
	$\gamma_{3,4}$	0.35	0.46

TABLE II
DEMODULATION RESULTS DURING MAKAIEX

Source-receiver range		20 m	80 m	160 m	290 m	430 m	900 m	1080 m
Single vector sensor	output MSE	-13.9 dB	-8.4 dB	-4.7 dB	Fail	-3.9 dB	-4.6 dB	-4.1 dB
	BER	BER=0	BER=4e-4	BER=0.03	BER=0.15	BER=0.05	BER=0.02	BER=0.04
Pressure sensor array	output MSE	-8.4 dB	-5.9 dB	Fail	-4.8 dB	-5.3 dB	Fail	Fail
	BER	BER=5e-5	BER=0.01	BER=0.14	BER=0.02	BER=0.01	BER=0.18	BER=0.24
Vector sensor array	output MSE	-13.2 dB	-11.9 dB	-8.3 dB	-6.3 dB	-6.7 dB	-4.6 dB	-4.0 dB
	BER	BER=0	BER=0	BER=2e-3	BER=8e-3	BER=3e-3	BER=0.03	BER=0.04

TABLE III
MEASURED CHANNEL CHARACTERISTICS DURING MAKAIEX

Range		20 m	80 m	160 m	290 m	430 m	900 m	1080 m
RMS delay spread for one vector sensor (ms)	CH#1	3.7	4.6	5.6	7.5	7.2	3.8	3.8
	CH#2	3.8	4.6	4.6	7.3	6.2	4.2	4.1
	CH#3	2.0	3.5	4.1	7.2	6.5	4.1	4.1
	CH#4	2.6	3.7	4.9	7.9	7.1	4.2	4.6
Average channel correlation for one vector sensor	$\bar{\gamma}_{1,2}$	0.68	0.83	0.72	0.67	0.51	0.74	0.75
	$\bar{\gamma}_{1,3}$	0.84	0.86	0.79	0.75	0.49	0.67	0.68
	$\bar{\bar{\gamma}}_{1,4}$	0.88	0.76	0.50	0.38	0.64	0.78	0.78
	$\bar{\gamma}_{2,3}$	0.73	0.85	0.85	0.80	0.79	0.95	0.79
	$\bar{\gamma}_{2,4}$	0.65	0.68	0.60	0.43	0.78	0.72	0.73
	$\bar{\gamma}_{3,4}$	0.92	0.92	0.79	0.66	0.71	0.59	0.57
RMS delay spread for pressure sensor array (ms)	CH#1	3.7	4.6	5.6	7.5	7.2	3.8	3.8
	CH#2	4.6	5.1	5.4	7.8	6.4	3.8	3.8
	CH#3	4.9	4.9	5.4	7.8	6.6	3.9	3.9
	CH#4	4.8	5.1	5.2	7.8	6.5	3.8	3.9
Average channel correlation for pressure sensor array	$\bar{\gamma}_{1,2}$	0.70	0.82	0.61	0.33	0.83	0.99	0.98
	$\bar{\gamma}_{1,3}$	0.53	0.80	0.63	0.62	0.59	0.96	0.93
	$\bar{\gamma}_{1,4}$	0.59	0.59	0.68	0.43	0.70	0.94	0.89
	$\bar{\gamma}_{2,3}$	0.84	0.81	0.63	0.39	0.73	0.98	0.96
	$\bar{\gamma}_{2,4}$	0.74	0.74	0.61	0.52	0.69	0.96	0.92
	$\bar{\gamma}_{3,4}$	0.91	0.86	0.73	0.40	0.70	0.98	0.96